

# Microtubules support a disk-like septin arrangement at the plasma membrane of mammalian cells

Mikael E. Sellin, Per Holmfeldt\*, Sonja Stenmark, and Martin Gullberg

Department of Molecular Biology, Umeå University, SE-901 87 Umeå, Sweden

**ABSTRACT** Septin family proteins oligomerize through guanosine 5'-triphosphate-binding domains into core heteromers, which in turn polymerize at the cleavage furrow of dividing fungal and animal cells. Septin assemblies during the interphase of animal cells remain poorly defined and are the topic of this report. In this study, we developed protocols for visualization of authentic higher-order assemblies using tagged septins to effectively replace the endogenous gene product within septin core heteromers in human cells. Our analysis revealed that septins assemble into microtubule-supported, disk-like structures at the plasma membrane. In the absence of cell substrate adhesion, this is the predominant higher-order arrangement in interphase cells and each of the seven to eight septin family members expressed by the two analyzed cell types appears equally represented. However, studies of myeloid and lymphoid cell model systems revealed cell type-specific alterations of higher-order septin arrangements in response to substrate adhesion. Live-cell observations suggested that all higher-order septin assemblies are mutually exclusive with plasma membrane regions undergoing remodeling. The combined data point to a mechanism by which densely arranged cortical microtubules, which are typical for nonadhered spherical cells, support plasma membrane-bound, disk-like septin assemblies.

## Monitoring Editor

Douglas R. Kellogg  
University of California,  
Santa Cruz

Received: Sep 6, 2011

Revised: Sep 26, 2011

Accepted: Oct 4, 2011

## INTRODUCTION

Septins comprise a family of guanosine 5'-triphosphate (GTP)-binding proteins implicated in membrane compartmentalization, cell polarity, and cytokinesis in fungal and animal cells (reviewed in Oh and Bi [2011]). The deciphering of molecular mechanisms has been hampered by the multitude of septin genes, with seven in most yeast species and nine to 17 in vertebrates (Pan *et al.*, 2007). Animal

septin family members fall into independent evolutionary groups (Kinoshita, 2003b). Mammals have 13 genes encoding both ubiquitous and tissue-specific septins (SEPT1-12, and SEPT14 in humans, note that the former *SEPT13* is pseudogene *SEPT7P2*), which have been classified into four homology subgroups named for the founding members SEPT2, SEPT3, SEPT6, and SEPT7 (Kinoshita, 2003a). All four subgroups appear to be represented in vertebrates but not in animals belonging to nonchordate phyla (Cao *et al.*, 2007).

Septins assemble into core heteromer units, which in turn serve as building blocks of higher-order structures (reviewed in Weirich *et al.* [2008]). When coexpressed in *Escherichia coli*, human SEPT2, SEPT6, and SEPT7 assemble into apolar six-subunit rods, arranged as a dimer of trimers with SEPT7 at the ends. In a manner similar to authentic core heteromers, these six-subunit rods polymerize into filaments at low ionic strength (Sheffield *et al.*, 2003; Sirajuddin *et al.*, 2007). Recombinant coexpression of four specific septins of budding yeast has resulted in the characterization of a cognate eight-subunit core heteromer arranged as a perfect palindrome (Bertin *et al.*, 2008). Crystals of bacterially expressed human septins have identified universal oligomerization interfaces—denoted as the G-interface and the NC-interface—that are located on opposite sides of the conserved GTP-binding domain (G-domain). These

This article was published online ahead of print in MBoC in Press (<http://www.molbiolcell.org/cgi/doi/10.1091/mbc.E11-09-0754>) on October 12, 2011.

\*Present address: Department of Oncology, St. Jude Children's Research Hospital, Memphis, TN 38105.

Address correspondence to: Mikael E Sellin ([mikael.sellin@molbiol.umu.se](mailto:mikael.sellin@molbiol.umu.se)).

Abbreviations used: AcGFP, *Aequorea coerulescens* green fluorescent protein; BSA, bovine serum albumin; EBV, Epstein-Barr virus; G-domain, GTP-binding domain; GTP, guanosine 5'-triphosphate; His-SEPT7, His-tagged SEPT7; Op18, Oncoprotein 18/Stathmin; MAP4, microtubule-associated protein 4; SEPT2-FLAG, SEPT2 derivative with an 8-amino acid FLAG; shRNA, short-hairpin RNA; TBCE, tubulin binding cofactor E; WGA, wheat germ agglutinin; YFP, yellow fluorescent protein.

© 2011 Sellin *et al.* This article is distributed by The American Society for Cell Biology under license from the author(s). Two months after publication it is available to the public under an Attribution-Noncommercial-Share Alike 3.0 Unported Creative Commons License (<http://creativecommons.org/licenses/by-nc-sa/3.0>).

"ASCB®," "The American Society for Cell Biology®," and "Molecular Biology of the Cell®" are registered trademarks of The American Society of Cell Biology.

interfaces mediate assembly into both core heteromers and extended filaments (Sirajuddin *et al.*, 2007, 2009).

All the essential functions of septins in budding yeast depend on filament formation (McMurray *et al.*, 2011). Moreover, septins bind phosphatidylinositol-4,5-bisphosphate (PIP<sub>2</sub>; Zhang *et al.*, 1999; Casamayor and Snyder, 2003), which may direct filament formation onto the inner leaflet of the plasma membrane (Tanaka-Takiguchi *et al.*, 2009; Bertin *et al.*, 2010). In budding yeast, septins assemble into elaborate lateral diffusion barriers and molecular scaffolds at the bud neck (reviewed in Caudron and Barral [2009]). These higher-order filamentous arrangements are dynamically modified through each cell division cycle and involve both longitudinal and lateral interactions between heteromers. At cell cycle entry, septins establish polarity by forming a ring-like structure at the incipient bud site, which is rearranged into an hourglass-shaped collar around the emerging bud neck, which is followed by the “hourglass-to-split rings” transition during cytokinesis. This transition involves rapid disassembly of paired filaments running parallel to the growth axis, which is followed by reassembly perpendicular to the growth axis (Vrabioiu and Mitchison, 2006; DeMay *et al.*, 2011). While the best understood septin arrangement by far is that of filaments at the fungal bud neck, septins localize to the cleavage furrow during cytokinesis in all cell types across kingdoms, which suggests a conserved role during late stages of cell division (Caudron and Barral, 2009).

Mammalian septins have been ascribed diverse roles during the interphase of the cell cycle, including DNA damage response, chromosome segregation, and exocytosis, as well as tumor and neurological disease states (reviewed in Peterson and Petty [2010]). Consistent with compartmentalization of the plasma membrane, septins have been shown to localize to the annulus of spermatozoa and at the base of cell appendages, such as cilia and neural spines (Ihara *et al.*, 2005; Kissel *et al.*, 2005; Tada *et al.*, 2007; Xie *et al.*, 2007; Hu *et al.*, 2010). Mammalian septins have been reported to associate to locations at the cell cortex, as well as to actin bundles, phagocytic vesicles, and/or microtubules (Kinoshita *et al.*, 2002; Surka *et al.*, 2002; Nagata *et al.*, 2003; Vega and Hsu, 2003; Martinez *et al.*, 2006; Huang *et al.*, 2008). Septins may also form free-floating cytoplasmic rings shortly after drug disruption of actin bundles (Kinoshita *et al.*, 2002). It is also noteworthy that individual septins have been assigned a diverse array of scaffolding functions at locations distal from the cell cortex (Kremer *et al.*, 2005, 2007; Spiliotis *et al.*, 2005; Mostowy *et al.*, 2010). Thus the links between higher-order filamentous assemblies and proposed septin functions in interphase or postmitotic mammalian cells remain poorly understood.

Most mammalian cells express a tissue-specific collection of multiple members and/or isoforms of each of the SEPT2, SEPT3, and SEPT6 subgroups, but a single subgroup member, SEPT7, appears expressed in all cell types (Cao *et al.*, 2007). This has evoked questions concerning the degree of combinational diversity and whether homology-based subgroups predict septin-pairing preferences. By analyzing human cell lines lacking or overexpressing selected septins, we have recently derived a generic model for how subgroup-specific properties direct the subunit arrangement within heteromers (Sellin *et al.*, 2011). That study suggested that individual septins exist solely in the context of stable six- to eight-subunit core heteromers, all of which contain variable SEPT2- and SEPT6-subgroup members together with SEPT7. The subpopulation of eight-subunit heteromers was found to also contain SEPT9—the sole SEPT3-subgroup member expressed by the analyzed cell types. Thus native septin filaments are predictively built from an array of core heteromers, all of which contain SEPT7, and with the variable septin subunits arranged according to

subgroup (see Figure 1A, a model in part based on Sirajuddin *et al.* [2007])

In this paper, we describe essential premises for live-cell imaging of the septin system in mammals. Our approach involved stably expressed *Aequorea coerulescens* green fluorescent protein (AcGFP)-fusion derivatives of septins belonging to each one of the four homology subgroups. We noted many caveats of septin-AcGFP reporters, such as an aberrant heteromeric context and formation of ectopic filaments. However, by optimizing conditions for effective replacement of endogenous SEPT7 with SEPT7-AcGFP within heteromers, we achieved specific visualization of various types of heteromer assemblies. Our data, combined with previous studies, suggest a general model for assembly of higher-order septin arrangements at the locations providing the greatest opportunity for binding cooperativity, which depends on both the cell type and external cues.

## RESULTS

### Septin core heteromers do not exchange their subunits

As outlined in the *Introduction*, individual septins in human cell lines appear to exist solely in the context of six- to eight-subunit heteromers in which the subunit arrangement coincides with homology-based subgroups (see Figure 1A). To address whether preexisting heteromers exchange their septin subunits, the heteromeric context of expressed His-tagged SEPT7 (His-SEPT7) was analyzed over time. For regulatable expression in stably transfected human cells, we used the episomally replicating pMEP vector system and the K562 erythroleukemia cell line. By initial suppression followed by induction, a transient burst of expression from the hMTIIa promoter can be achieved (Melander Gradin *et al.*, 1997; Sellin *et al.*, 2008a). Western blots showed inducible expression of His-SEPT7, which migrates above endogenous SEPT7 due to a His tag (Figure 1B). Quantification of Western blots showed that the total amounts of soluble SEPT7 protein—that is, His-SEPT7 (shaded bars) together with endogenous SEPT7 (open bars)—was transiently increased three- to fourfold within 4 h of induction (Figure 1C).

Artificially expressed SEPT7 is known to form insoluble aggregates (Kinoshita, 2003a; Sheffield *et al.*, 2003), which we confirmed by boiling insoluble proteins in SDS sample buffer. Western blotting revealed insoluble His-SEPT7 between 4 and 72 h after the induced burst of expression, but not at the final time point on day 4 (Supplemental Figure S1). Thus, at most time points only about one-half of the expressed His-SEPT7 protein is soluble, but insoluble His-SEPT7 aggregates appeared essentially degraded after 4 d.

It is evident from Figure 1, B and C, that induced His-SEPT7 expression caused a gradual decline of the endogenous gene product, while SEPT2, SEPT6, and SEPT9 remained constant. This is consistent with excess His-SEPT7 competing for limited amounts of heterooligomerization partners, and with the nonheteromeric SEPT7 protein being unstable, as previously found (Sellin *et al.*, 2011). Given that K562 cells double approximately every 20 h, endogenous SEPT7 declined at a rate compatible with dilution by newly synthesized and successfully heterooligomerized His-SEPT7 during each cell division. This suggests that the core heteromer assembly process is cotranslational and irreversible.

To determine the heteromeric context of His-SEPT7 over time, we fractionated crude cell extracts by density-gradient centrifugation. High-salt cell extraction buffers and gradients were prepared that disassembled all higher-order septin structures in K562 cells into pools of soluble six- to eight-subunit heteromers (Sellin *et al.*, 2011). By this means, the fraction of His-SEPT7 containing heteromers could be determined. Figure 1D shows that the initial accumulation

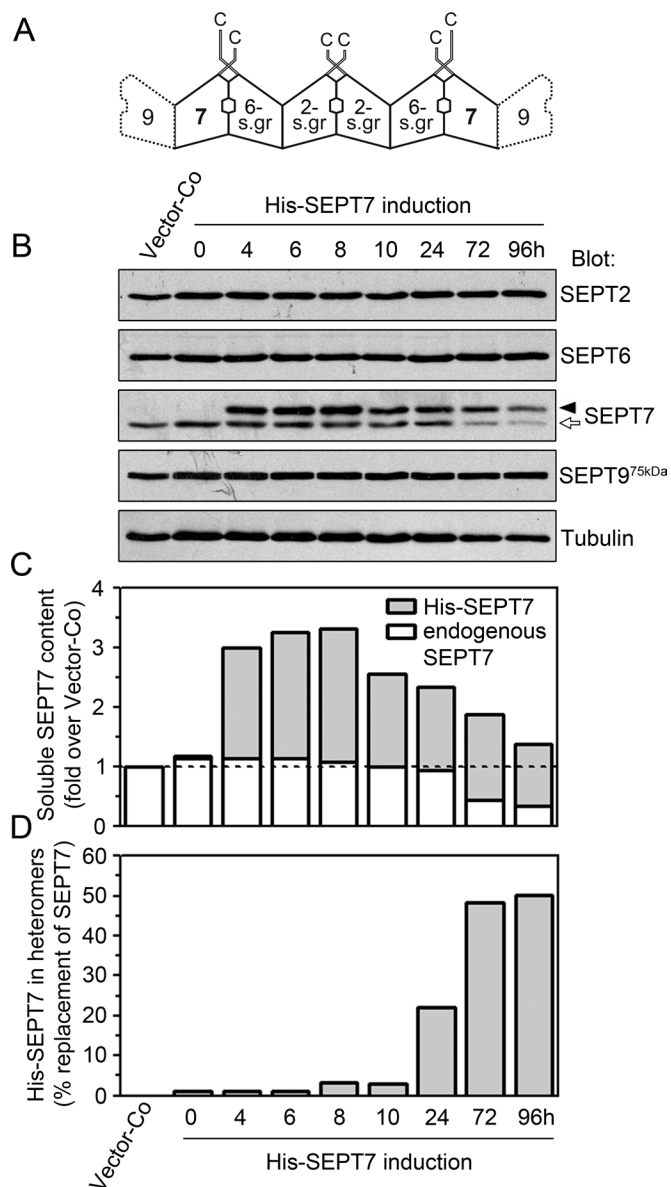


**FIGURE 1:** Analyses of endogenous septins and core heteromers in cells induced to express a transient burst of the epitope-tagged His-SEPT7. (A) Depiction of the repertoire of hexameric and octameric core heteromers in K562 cells. The arrangement of SEPT2 subgroup (2-s.g.r: SEPT2 and SEPT5) and SEPT6 subgroup (6-s.g.r: SEPT6, SEPT8, and SEPT11) members, as well as SEPT7, is according to the solved structure of a recombinant head-to-head SEPT2/6/7 trimer (PDB ID 2qag). The octamers are depicted with SEPT9 at their ends; however, it remains possible that these are arranged with a SEPT9 dimer at one end. (B) K562 cells were transfected with a shuttle vector directing inducible expression of His-SEPT7 or an empty vector (Vector-Co), and counterselected with hygromycin, and expression was controlled as outlined in *Material and Methods*. Crude extracts were prepared at the indicated time after induced expression and cleared by high-speed centrifugation, and soluble proteins were analyzed by Western blotting using the indicated antibodies ( $\alpha$ -tubulin: loading control). An open arrow indicates the endogenous SEPT7 protein and an arrowhead indicates His-SEPT7. (C) The relative content of endogenous SEPT7 (open part of the bar) and His-SEPT7 (filled part of the bar) was determined at each time point by quantification of Western blots (the endogenous SEPT7 level in Vector-Co = 1). (D) The percentage of core heteromers containing His-SEPT7 was determined by density-gradient centrifugation at various time points followed by Western blotting of SEPT7 in fractions sedimenting between 6.5 and

of soluble His-SEPT7 (i.e., between 4 and 6 h) did not result in replacement of endogenous SEPT7 within the preexisting heteromer pool. However, a gradual replacement was evident over the 96-h time course, which confirms that His-SEPT7 competes successfully during de novo heterooligomerization.

The data in Figure 1 were faithfully reproduced by analyses of SEPT2, SEPT6, and SEPT7 containing a C-terminal FLAG epitope tag (unpublished data). Thus we found no evidence for subunit exchange within preexisting heteromers, which suggests that core heteromers are essentially stable protein complexes.

### Differential assembly states of expressed AcGFP-tagged, homology-based subgroup representatives

The above data show that unbalanced septin expression may result in aggregation and that a tagged septin derivative cannot be expected to become incorporated into preexisting heteromers. Thus live-cell imaging of the septin system requires fluorescent septin reporters to be expressed at modest levels over many cell doublings. Accordingly, the fluorescent reporters analyzed in Figure 2, which includes a representative of each of the four septin homology-based subgroups tagged at the C-terminus with AcGFP, were expressed by the low basal activity of the hMTIIa promoter of the replicating pMEP vector over a time period corresponding to at least seven cell doublings. Under these circumstances, the contents of SEPT2-, SEPT6-, SEPT7- and SEPT9-AcGFP in cleared lysates of the transfected K562 cell lines appear roughly the same (Figure 2A).

On the basis of mRNA analysis of all septin family members, we have found that K562 cells express significant levels of seven endogenous septins (Sellin *et al.*, 2011). As indicated in Figure 2A, these include two and three members of the SEPT2 and SEPT6 subgroup, respectively. It is noteworthy that SEPT6-AcGFP expression caused a decreased content of all the endogenous SEPT6 subgroup members, that is, SEPT6/8/11, while other septins remained unaltered. Moreover, SEPT7-AcGFP expression caused a selective decrease of the single subgroup member SEPT7. Consistent with our previous report (Sellin *et al.*, 2011), these data suggest subgroup-restricted competition for limiting amounts of heterooligomerization partners. However, expression of SEPT2-AcGFP or SEPT9-AcGFP had little or no effect on the levels of any of the endogenous septins (Figure 2A), which suggests unsuccessful competition with the cognate endogenous septins.

Endogenous septins appear to exist solely in the context of six- to eight-subunit heteromers (Sellin *et al.*, 2011), which are resolved as a single peak by the present density-gradient centrifugation protocol (note coinciding peaks in Figure 2B). On the basis of detection of representatives of each of the four homology subgroups, as well as the AcGFP-reporter, we found that heteromers derived from SEPT7-AcGFP-expressing cells sedimented similarly to heteromers in untransfected control cells, that is, as single overlapping peaks (compare Figure 2, B and E; note that a 26.9-kDa AcGFP reporter is too small to alter heteromer peak positions). In contrast, however, other AcGFP-tagged septins also exist in a nonheteromeric context and SEPT9-AcGFP (Figure 2F) almost completely failed to assemble with endogenous septins. The hydrodynamic parameters (i.e., the Stokes' radius and sedimentation coefficient, as described in Sellin *et al.* [2011]) of the nonheteromeric forms indicate that SEPT2-AcGFP exists as a homodimer, while SEPT6- and SEPT9-AcGFP exist as monomers (unpublished data).

10S, which includes both six- and eight-subunit septin heteromers. The replacement percentage was calculated based on the ratio between endogenous SEPT7 and His-SEPT7.

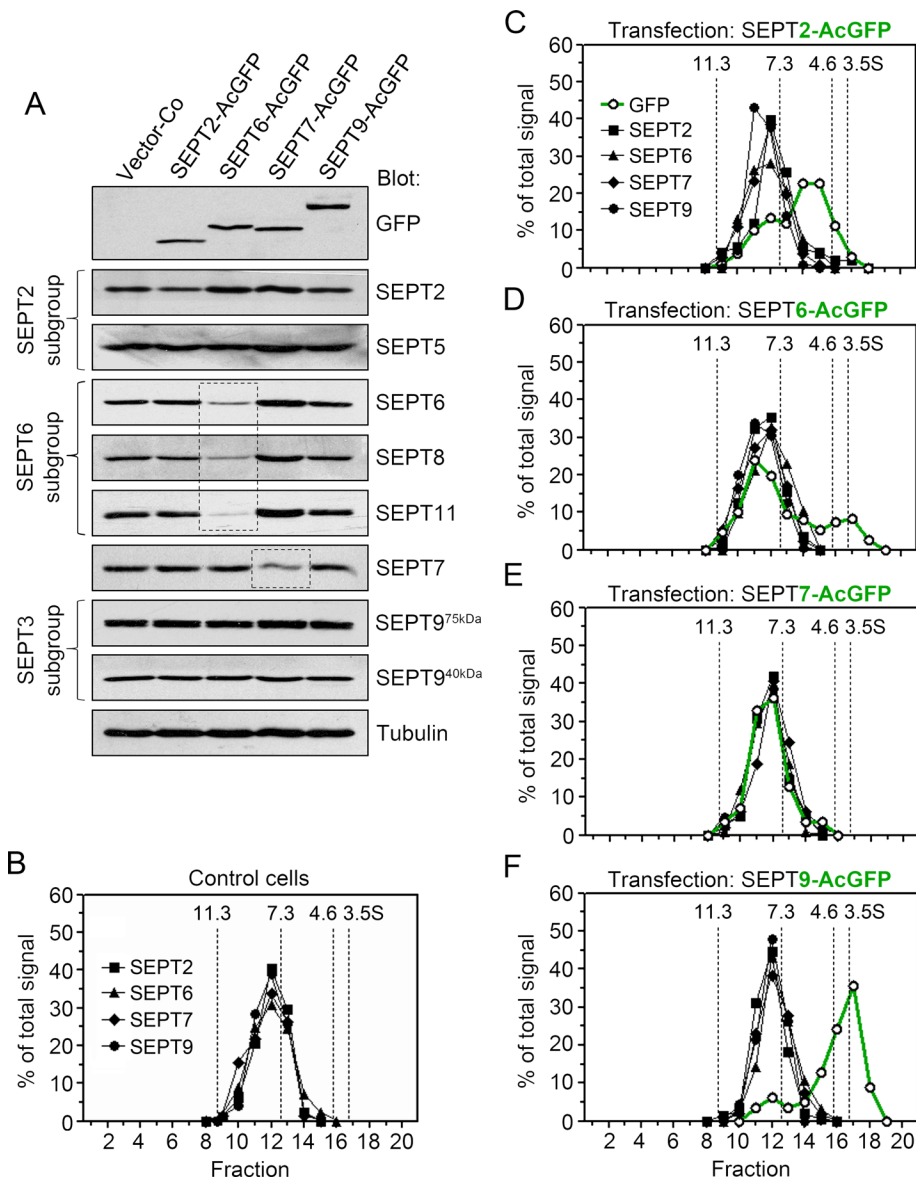


**FIGURE 2:** Evaluation of the septin system in cell lines stably expressing septin-AcGFP reporters representing each of the four homology-based subgroups. K562 cells were transfected with pMEP4-based shuttle vectors directing expression of the indicated septin-AcGFP reporter and counterselected as outlined in *Materials and Methods* (note that the expressed SEPT9 isoform corresponds to the *v1*-transcript). Expression corresponds to the basal activity of the hMTIIa promoter. (A) Crude cell extracts were prepared and analyzed by Western blotting, as in Figure 1B. The analyses include all seven septins significantly expressed in K562 cells; their homology-based subgroups are indicated on the left. Isoforms of SEPT9 migrating close to the predicted SEPT9<sub>v1</sub> isoform at 75 kDa are all termed SEPT9<sup>75 kDa</sup>, and the isoform migrating at 40 kDa is termed SEPT9<sup>40 kDa</sup>. (B to F) Crude extracts prepared from the indicated cell lines were resolved by density-gradient centrifugation. The distribution of endogenous and AcGFP-tagged septins in fractions was analyzed by Western blot analysis using the indicated antibodies. For SEPT9, the 75 kDa and 40 kDa isoforms were indistinguishable in their distribution. Note that six- and eight-subunit heteromers are not resolved under these conditions. Sedimentation peaks for proteins of known S values are indicated by vertical dotted lines.

Figure 2 shows that AcGFP-fused septin derivatives differ in their proficiency in competing with cognate endogenous septins for heterooligomerization partners, as well as in their persistence in a non-heteromeric context. According to these data, only SEPT7-AcGFP qualifies as a bona fide specific reporter of the localization of endogenous core heteromers.

### Cortical disk-like structures are predominant septin assemblies during interphase of a nonadherent cell type

SEPT7 is the sole member of its subgroup and is present in all native heteromers. Hence SEPT7-AcGFP can be expected to visualize the complete core heteromer pool without altering the composition of other septins. Epifluorescence analysis of the SEPT7-AcGFP-expressing K562 cell line described in Figure 2 revealed localization of septin assemblies that seemed consistent with immunostaining of SEPT7 in methanol-fixed, nontransfected cells, but with superior resolution and sensitivity (Figure 3, A and B). Thus SEPT7-AcGFP localized mainly to the cleavage furrow during cytokinesis and appeared as distinct cortical assemblies in interphase cells. In contrast, the other AcGFP-reporters described in Figure 2 were prone to form ectopic filaments and aggregates, and/or appeared as nonlocalized in the cytosol (Figures S2 and S3).

Previous reports on septin localization have focused on adhesion substrate-dependent cell types. However, K562 cells lack functional integrins on the surface and are consequently nonadherent and have a uniform spherical shape (Muller *et al.*, 1995), which provides spatial separation across the cortex. This simplified characterization of cortical septin assemblies, which were the predominant higher-order septin arrangement detected in interphase cells. Optical sectioning of live cells revealed disk-like submembranous structures (compare the section at the cell equator with the section parallel to the plasma membrane in Figure 3B). These structures appear less distinct in fixed and immunostained cells (compare Figure 3, A and B). Inspection of live cells revealed a central clearing in many of the disk-like structures (see enlargement in Figure 3B and intensity profiles in Figure S4A), that is consistent with closed septin filaments. The disk-like structures appeared uniformly sized ( $\phi \sim 0.8 \mu\text{m}$ ; Figure 3C), and optical sectioning of interphase cells suggested an even cortical distribution (Figure S4B). Based on analysis of consecutive optical sections, the number of disk-like structures was estimated to be  $141 \pm 29$  per cell (Figure S4C).

A disk-like septin arrangement with a central clearing appeared predominant among asynchronously proliferating K562 cells. Even so, some interphase cells displayed cortical septin assemblies appearing as less-defined patches (unpublished data). It is also noteworthy that, while septins did not detectably localize to the mitotic spindle of K562 cells and remained at the cortex until telophase, septin assemblies during metaphase did not appear as uniform as in interphase cells (Figure S4D). These observations are

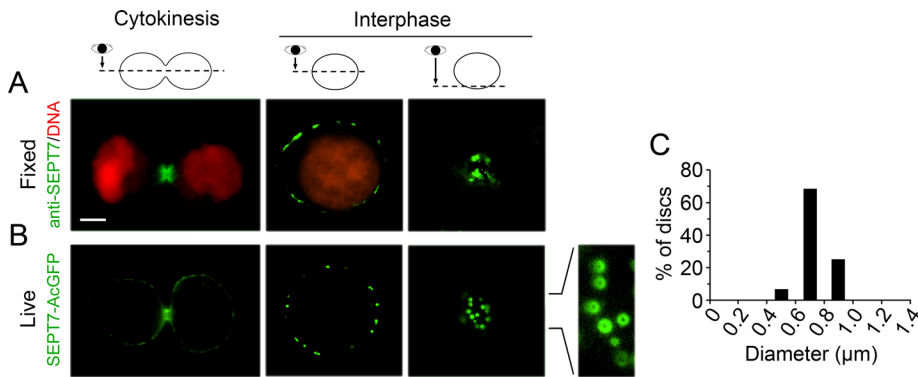


**FIGURE 3:** The localizations of endogenous core heteromers and SEPT7-AcGFP in nonadherent K562 cells. (A) Cells were methanol-fixed and immunostained with anti-SEPT7 (green). DNA was stained by propidium iodide (red). (B) Live SEPT7-AcGFP-expressing cells were generated as in Figure 2. Images (epifluorescence, 1000 $\times$  magnification) show representative cells during cytokinesis and interphase. Deconvoluted optical sections at either the equatorial plane or parallel to the plasma membrane, as indicated at the top, are shown. Scale bar: 5  $\mu$ m. (C) The diameters of the disk-like structures that are predominant in SEPT7-AcGFP-expressing cells were determined using the Olympus CellR imaging station software (122 septin disks total in 15 cells; 15- $\mu$ m fluorescent beads were used for calibration). The results are representative of five independent SEPT7-AcGFP-expressing K562 cell lines.

consistent with septin filament rearrangement prior to cytokinesis and the gradual reassembly of cortical disk-like structures after each cell division.

The present evaluation of reporter systems for imaging of septins in human cells revealed several examples of maladies associated with artificially expressed septin-fusion derivatives, which are discussed in the description of the data in Figures S2 and S3. However, our protocol for effective replacement of endogenous SEPT7 with SEPT7-AcGFP provides a system that fulfills the essential criteria of a specific reporter system. This facilitated detection of uniformly sized structures that, because of the impression of disks attached flat against the plasma membrane, are hereafter referred to as “septin disks.”

### The stability of septin disks is dependent on intact microtubules

In most cell types, septin assemblies appear to localize in conjunction with the plasma membrane, but cytosolic localization in association to actin bundles and/or microtubules has also been reported. Interphase K562 cells are spherical and have a dense array of microtubules that extend all along the cortex (optical sections at either the equatorial plane or parallel to the plasma membrane are shown in Figure 4A, Control). Moreover, filamentous actin localizes to both the cortex and cytosolic structures surrounding the Golgi apparatus (Figure S5). Still, we detected localization of septins to punctuate cortical assemblies only in interphase K562 cells (Figures 3 and S4). Interestingly, we found that nocodazole-mediated depolymerization of microtubules caused a gradual disintegration of these septin assemblies (Figure 4). As a consequence, most cells did not display any clearly resolved punctuate assemblies after 30 min, and septins appeared relatively evenly distributed at the cortex at this stage. A view perpendicular to the plasma membrane gave an impression of a diffuse array of minute septin assemblies (unpublished data), which suggests that most core heteromers at the cell cortex retain some higher-order filamentous structure.

Mammalian microtubules are renowned to be unstable at low temperatures and, similar to nocodazole treatment, cooling on ice

was found to cause both microtubule depolymerization and disintegration of septin disks (Figure 4A). Under these conditions, the septins also remained localized at the cell cortex. For comparison, cytochalasin D-treated K562 cells were also analyzed and showed that septin disks remain intact after disruption of the filamentous actin that surrounds the cortex (Figure S5). Thus microtubules, but not filamentous actin, are essential for septin disks at the cell cortex of nonadherent K562 cells.

To explore the interdependency of the microtubule and septin systems, K562 cells were depleted of their respective protomer units. Our experimental strategies relied on Epstein-Barr virus (EBV)-based replicating vectors directing expression of either a short-hairpin RNA (shRNA) targeting SEPT7 mRNA (shRNA-SEPT7) or a cDNA encoding the tubulin heterodimer disrupting protein cofactor E (pMEP-TBCE-FLAG; Bhamidipati *et al.*, 2000). All native heteromers in K562 cells contain SEPT7, and we have found that

SEPT7 depletion results in unstable aberrant complexes of SEPT2- and SEPT6-subgroup members and monomeric SEPT9 (Sellin *et al.*, 2011). Consistent with that report, Figure 5A shows that 1 wk of shRNA-SEPT7 expression depletes >90% of SEPT7; this depletion was associated with decreased content of all other septins, as would be anticipated. However, analyses of microtubule content and stability in these cells did not reveal any effects of septin depletion (note indistinguishable nocodazole dose responses in Figure 5B), which contrasts to shRNA-mediated depletion of either of the two well-characterized microtubule regulatory proteins oncoprotein 18/Stathmin (Op18) or microtubule-associated protein 4 (MAP4; Figure S6). We also analyzed consequences of artificial overexpression, but observed no effect of excessive septin levels on microtubules (Figure S7). In contrast, depletion of tubulin heterodimers, as observed within 8 h of induced TBCE expression (Figure 5C), resulted in complete disintegration of punctuate cortical septin assemblies in most cells (Figure 5D). Thus, while confirming the microtubule dependence of septin disks, the present data do not hint at a reciprocal dependency.

### Microtubule stabilization preserves septin disks in permeabilized cells

The microtubule-stabilizing drug Taxol promotes rapid polymerization, as well as a gradual accumulation of large microtubule bundles in K562 cells (Holmfeldt *et al.*, 2002). Figure 6A shows that Taxol rapidly increased the fraction of polymerized tubulin heterodimers in K562 cells to nearly 100%. In observing SEPT7-AcGFP localization in Taxol-treated cells, we did not note any clear-cut, immediate effects (Figure 6B, 3 min Taxol), but a gradual clustering of septin disks to one side of the spherical cortex became noticeable within 60 min (Figure 6B, 60 min Taxol). Thereafter, an increasing fraction of cells appeared in which all SEPT7-AcGFP was localized to elongated structures (Figure 6, A and B, 4 h Taxol). Co-staining of tubulin revealed that these obviously aberrant structures consisted of the extensive microtubule bundles that gradually form during prolonged Taxol treatment (Figure S8). This is indeed consistent with septin localization to microtubule bundles in Taxol-treated epithelial cells (Bowen *et al.*, 2011), as well as localization to the circumferential

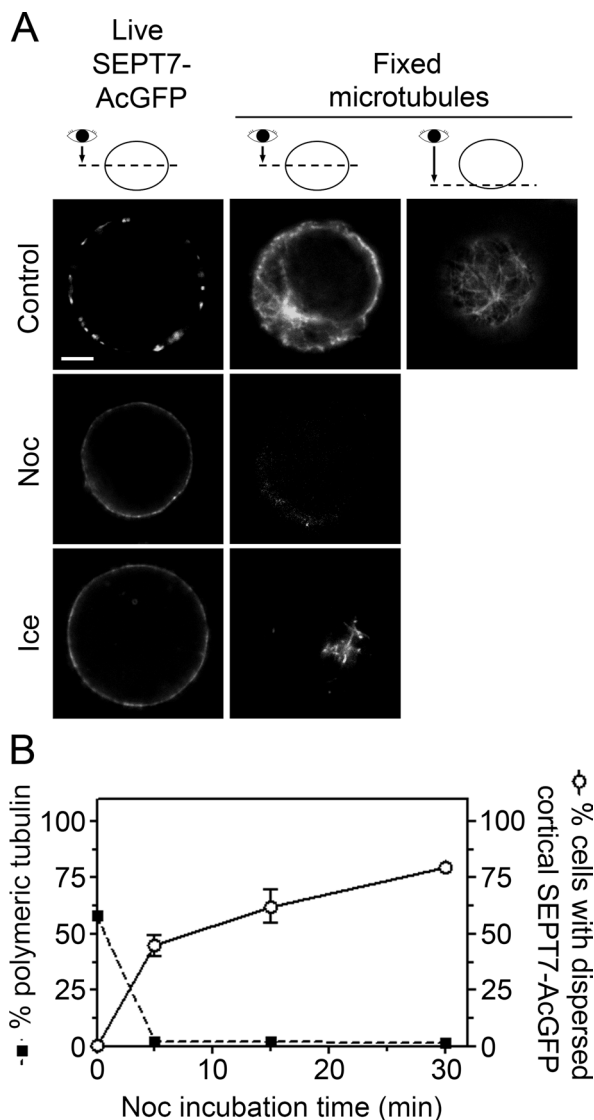


**FIGURE 4:** The dependency of septin disks on an intact microtubule system. (A) SEPT7-AcGFP-expressing K562 cells (generated as in Figure 2) were treated with nocodazole (Noc; 6  $\mu$ M for 30 min) or incubated for 15 min on ice. Left, deconvoluted optical sections at the equatorial plane of living cells and reveals the localization of SEPT7-AcGFP-labeled septin core heteromers. Right, the appearance of microtubules of fixed untransfected cells in which nonpolymeric tubulin heterodimers were extracted prior to fixation. Deconvoluted optical sections at either the equatorial plane or parallel to the plasma membrane, as indicated at top, are shown. Scale bar: 5  $\mu$ m. (B) The effect of nocodazole on the partitioning of tubulin heterodimers (■) was determined as outlined in *Materials and Methods* and expressed as percentage polymeric tubulin of the estimated total content of polymerization-competent tubulin. The appearance of septin assemblies after nocodazole addition was evaluated by observation of SEPT7-AcGFP-expressing K562 cells. In this cell population, >96% displayed uniform cortical septin assemblies, such as shown in Control in (A). The remaining 3–4% of all cells contained SEPT7-AcGFP aggregates and were excluded from the analysis. Individual interphase cells were evaluated using the criteria of complete dispersal of the punctate assemblies displayed by control cells (see images in (A)); ○, dispersed cortical). To minimize ambiguity, cells that still retained some of these assemblies were classified as nondispersed, i.e., punctate. The diagram represents the mean  $\pm$  SE of data from two independent experiments ( $n = 150$  cells for each time point; error bars indicate maximum and minimum values).

microtubule coil in platelets (Martinez *et al.*, 2006). Thus septins may have an innate affinity for microtubules (or associated proteins), which can be expected to gain in avidity with multiple-bond interactions on bundles.

Permeabilization of K562 cells at physiological ionic strength results in disassembly of both the microtubule and septin systems, and their respective protomer units are released into the media (Sellin *et al.*, 2011). To further address the microtubule dependence of septin disks, we analyzed the effect of a brief Taxol exposure prior to permeabilization of K562 cells. Epifluorescence analysis of permeabilized control cells showed the expected release of all cell-associated SEPT7-AcGFP, as well as tubulin (compare fixation prior or subsequent to permeabilization in Figure 7A, Control). Significantly, Taxol exposure prior to permeabilization not only resulted in the expected stabilization of microtubules, but also in preservation of septin disks (Figure 7A, 3 min Taxol).

Taxol-mediated preservation of septin disks in permeabilized cells provided a means for a semiquantitative analysis of their septin composition. Accordingly, K562 cells were permeabilized in the absence and presence of Taxol and the partitioning of individual septins between soluble (i.e., released) and insoluble (i.e., cell-associated) states was evaluated by Western blotting (Figure 7B). The data show that, while most tubulin was released by permeabilized nontreated cells, a brief Taxol exposure was sufficient for recovery of most tubulin in the cell-associated fraction. Significantly, while completely released by nontreated cells, ~50% of all septins were recovered in the cell-associated fraction in the presence of Taxol (Figure 7B). Quantification of Western blots by serial dilution of cell lysates suggested that all individual septins are indistinguishable with respect to their partitioning between soluble and insoluble states (Figure 7C).

The present data suggest that all septin family members contribute equally to microtubule-supported septin disks. In line with this notion, our analysis of cells depleted of selected septins (by means of shRNA vectors) failed to identify any individual septin of particular significance for microtubule-dependent stabilization of septin disks (Figure S9). Thus these microtubule-supported septin assemblies appear independent of the specific septin composition of K562 cells.

#### Punctuate cortical septin assemblies accumulate in the uropod during amoeboid movement

To address septin localization and dynamics in a physiological context, we used the SEPT7-AcGFP reporter in combination with the Jurkat cell line, which provides a well-characterized T-lymphocyte model system. Phase-contrast and fluorescence microscopy of albumin-plated, live Jurkat cells—that is, nonmotile control cells—revealed a spherical shape with uniformly sized punctuate septin assemblies (Figure 8A). Similar to K562 (Figures 3 and S4B), inspection parallel to the plasma membrane of interphase cells showed cortical  $\varnothing \sim 0.8\text{-}\mu\text{m}$  septin disks, which represent the predominant higher-order arrangement (Figure 8A). Moreover, analyses of permeabilized Jurkat cells confirmed that these septin assemblies are preserved by microtubule stabilization (Figure S10). Thus the  $\varnothing \sim 0.8\text{-}\mu\text{m}$  disk-like arrangement characterized in undifferentiated K562 cells is also predominant in a nonactivated differentiated cell type that grows in suspension.

Plating on invasin, an integrin-activating bacterial protein, stimulates polarization and amoeboid movement of T lymphocytes (Arenchibia *et al.*, 1997). Figure 8B, left, shows a phase-contrast image of a Jurkat cell migrating on an invasin-coated surface. Letters indicate the trailing uropod (U), which lacks substrate

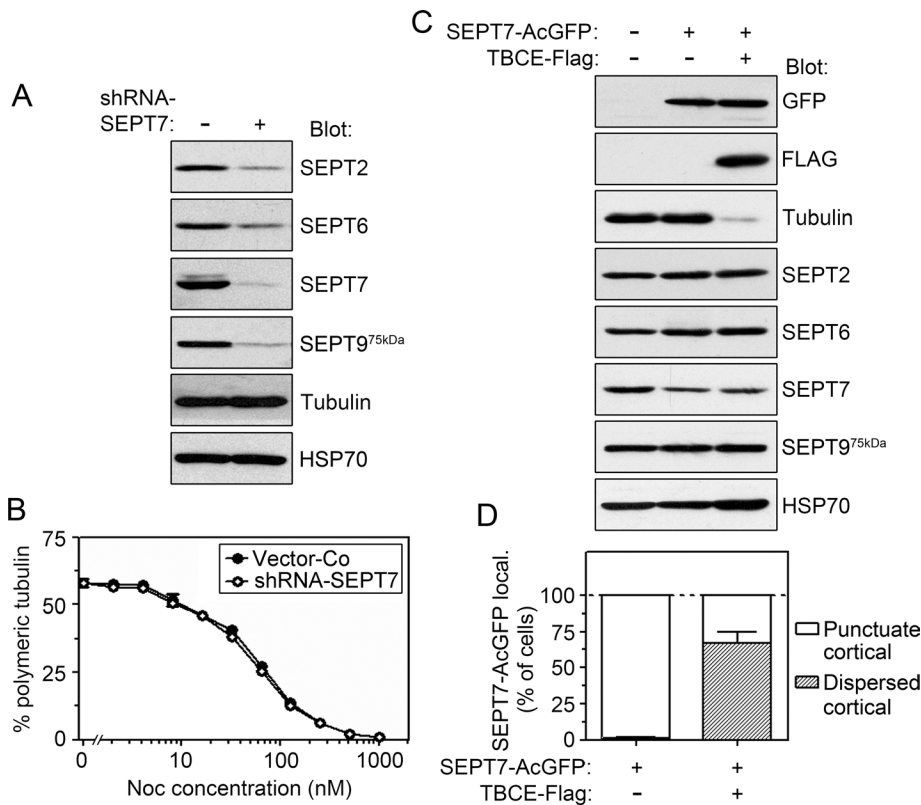


**FIGURE 5:** Evaluation of interdependencies between the microtubule and septin systems. (A) K562 cells were transfected with Vector-Co or an shRNA-SEPT7 shuttle vector and counterselected with hygromycin for 1 wk. Cell extracts were analyzed by Western blotting of representatives of each of the four septin subgroups, which revealed substantial depletion of all the analyzed septins (HSP70: loading control). (B) To assess potential effects of septin depletion on microtubule stability, Vector-Co and shRNA-SEPT7-expressing cells were treated for 30 min with graded concentrations of nocodazole. Partitioning of tubulin heterodimers was determined as in Figure 4B. (C) K562 cells were cotransfected with EBV-based replicating vectors directing constitutive expression of SEPT7-AcGFP (pCEP-SEPT7-AcGFP) and inducible expression of FLAG-tagged cofactor E (pMEP-TBCE-FLAG), as outlined in *Material and Methods*. Transfected cell lines were counterselected with hygromycin for 1 wk, and protein expression was induced for 8 h. Cell extracts were analyzed by Western blotting using the indicated antibodies (HSP70: loading control). (D) Disintegration of cortical septin assemblies was evaluated as in Figure 4B. The category denoted “punctuate cortical” also includes TBCE-expressing cells with reduced number of cortical punctuate septin assemblies. Bar charts represent the mean  $\pm$  SE of data from duplicate experiments.

attachment, and the substrate-attached pseudopodium (P) at the leading edge. The fluorescence image of the same cell reveals the absence of septin assemblies within the pseudopodium and accumulation of punctuate structures at the cortex of the uropod (a section across the uropod is shown in Figure 8B). Owing to being crowded in a confined area, septin assemblies cannot be readily distinguished as discrete structures. Inspections of optical sections did not provide any evidence for extended filaments in the uropod or at any other cellular locations (unpublished data).

Amoeboid movement is characterized by dynamic, actin-rich protrusions at the leading edge. To visualize actin dynamics, we used the actin filament-binding Lifeact peptide fused to DsRed monomer (Riedl *et al.*, 2008). Coexpression of this red fluorescence reporter with SEPT7-AcGFP confirms abundant actin filaments in pseudopodial protrusions at the leading edge, that is, spatially separated from the punctuate septin assemblies at the uropod cortex (Figure 8C). Scoring of individual protrusions in invasin-plated Jurkat cells revealed an essentially complete absence of protrusions

containing SEPT7-AcGFP fluorescence (Figure 8D). Thus, during amoeboid movement, regions characterized by dynamic actin polymerization and consequent plasma membrane remodeling appear mutually exclusive with higher-order septin structures, which accumulate at the cortex of the trailing uropod.

### Cell adhesion and spreading transforms septin disks into heterogeneous assemblies

K562 lacks cell surface  $\beta_1$  integrins, which can be amended by introducing an appropriate  $\alpha$  chain. To analyze the fate of septin disks after cell spreading on a surface coated with integrin-activating invasin, we therefore used K562 transfected with an integrin  $\alpha$ -8 chain (termed K562-KA8), which reconstitutes a functional integrin complex (Muller *et al.*, 1995). SEPT7-AcGFP-expressing K562-KA8 cells appeared indistinguishable from parental K562 with respect to spherical shape and even distribution of septin disks when plated on bovine serum albumin (BSA; unpublished data). However, K562-KA8 cells spread and become flattened if plated on invasin (Holmfeldt *et al.*, 2002). This is shown in Figure 9A, which presents a phase-contrast image, as well as an adhesion-substrate proximal section of a SEPT7-AcGFP-expressing K562-KA8 cell.

Inspection of septin assemblies revealed that the great majority of septin disks transformed into a variety of arrangements along cell edges and adjacent to the substrate attachment. The enlarged view in Figure 9A also shows that the punctuate assemblies were heterogeneous in size and shape, and in most cases smaller than the uniformly sized septin disks. Some of the punctuate assemblies had a central clearing, but these structures were also heterogeneous in size and shape (Figure S11). Thus septin assemblies in invasin-plated cells resembled the heterogeneous peripheral and punctuate septin arrangements previously described in adhesion substrate-dependent cell lines (reviewed in Lindsey and Momany [2006]).

K562-KA8 cells plated on an invasin-coated surface remained nonmotile, but had abundant filopodia at cell edges (see phase-contrast image in Figure 9A). These were continuously sprouting and readily visualized by a yellow fluorescent protein (YFP)-actin reporter, but inspection of individual filopodia in SEPT7-AcGFP-expressing cells revealed the absence of detectable septin assemblies (Figure 9B).

The pseudopodia of migrating Jurkat cells lacked septin assemblies at edges adjacent to the invasin attachment substrate, which contrasted to prominent septin assemblies along the edges of K562-KA8 cells (compare Figures 8 and 9). This may reflect that K562-KA8 cells are nonmotile and that extensive membrane remodeling is confined to locations of sprouting filopodia. To directly explore the relationship between membrane dynamics and the localization of

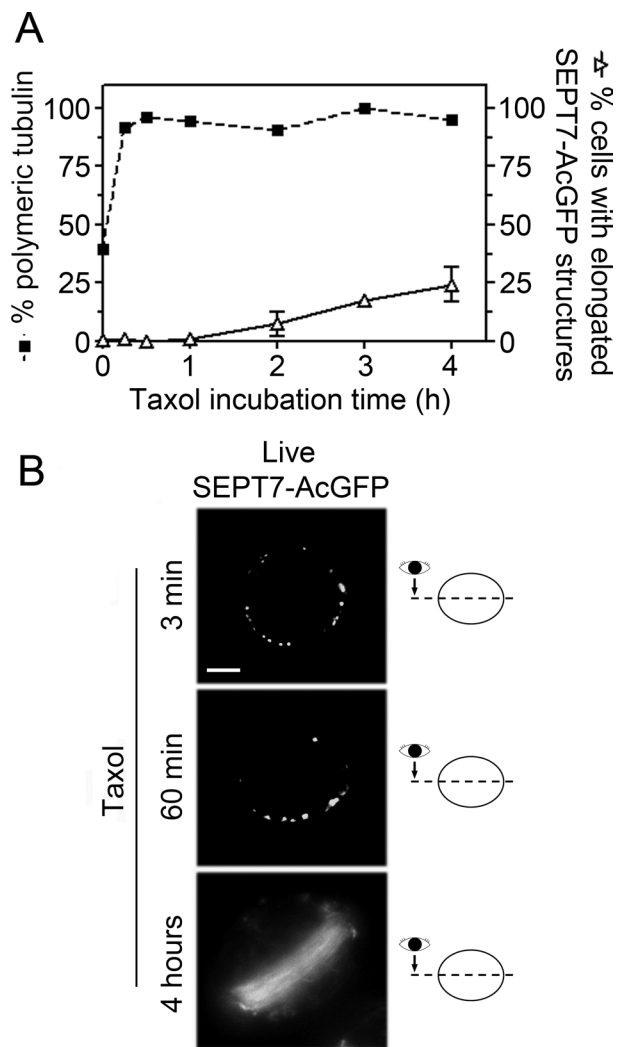


**FIGURE 6:** Consequences of Taxol-mediated microtubule stabilization and subsequent bundling for septin localization. (A) The effect of Taxol (3  $\mu$ M) on the partitioning of tubulin heterodimers (■) over a 4-h time course was determined as in Figure 4B. The appearance of septin disks after Taxol addition was evaluated by observations of live SEPT7-AcGFP-expressing K562 cells generated as in Figure 2. The first clear-cut alteration was a gradual clustering of septin disks to one side of the spherical cortex, which was evident in most cells within 30–60 min. Within 2 h, cells in which septins were entirely localized to elongated cytosolic structures (△) became easily recognizable. This genesis involved a gradual recruitment of clustered cortical septin disks, but the array of intermediate states was not classified as cytosolic structures. (B) Deconvoluted optical sections at the equatorial plane of representative SEPT7-AcGFP-expressing K562 cells treated with Taxol for 3 min and 60 min are shown, which illustrate the uneven cortical distribution of septin disks. The bottom panel shows a cell classified as having essentially all fluorescence localized to elongated cytosolic structures. Scale bar: 5  $\mu$ m.

higher-order septin filamentous structures, we studied K562-KA8 cells in which filopodia were visualized by labeling the outside of cells with a red fluorescence-labeled lectin. As is evident in the enlarged view in Figure 9C, the bases of filopodia were not surrounded by septins. Instead, it appears that filopodia only emerged at locations devoid of higher-order septin filamentous structures (note alternating green and filopodia-associated red fluorescence along the cell edge in the overlay shown in Figure 9C). Thus all the septin

arrangements observed upon invasion-plating of Jurkat and K562-KA8 cells appeared mutually exclusive with plasma membrane regions undergoing extensive remodeling.

### Septin disks appear excluded from endocytotic vesicles

For simultaneous visualization of septin disks and endocytosis via clathrin-coated pits in living cells, Alexa Fluor 594-labeled transferrin (red fluorescence) was added to SEPT7-AcGFP-expressing K562 cells. As expected, epifluorescence microscopy revealed continuous formation of endocytotic vesicles, and vesicles gathered at the area of the Golgi apparatus within a few minutes (Figure 10A). In contrast, septin disks were only detected at the cell cortex. As anticipated from the presented image, real-time observation of cells did not reveal any vesicles containing detectable SEPT7-AcGFP fluorescence (unpublished data).

To explore whether internalization of septin disks can be provoked by artificial clustering of an abundant transmembrane cell surface protein, we exposed K562 cells to anti-CD46 antibodies for 40 min, and then incubated them with cross-linking DyLight 549-labeled secondary antibodies at 37°C. Figure 10B shows that essentially all the secondary antibodies were residing in endocytotic vesicles within 30 min but, even under these cross-linking conditions, we only detected SEPT7-AcGFP fluorescence at the cell cortex. Thus septin assemblies were not under any circumstances detected in association with endocytotic vesicles.

### DISCUSSION

Previous reports on the organization of the mammalian septin system have focused on polarized and/or adhesion substrate-dependent cell types. This study examines two adhesion substrate-independent human cell model systems—the K562 myeloblastic/erythroblastic and the Jurkat T-lymphoblastic leukemia. In the absence of adhesion substrate attachment, these grow in suspension and lack actin bundles during interphase of the cell cycle. Under such conditions, microtubule-supported septin disks are the predominant higher-order septin arrangement, but these transform into a variety of arrangements upon cell spreading on an adhesion substrate. Moreover, all the septin arrangements observed in the present cell model systems appear mutually exclusive with plasma membrane regions undergoing remodeling. In this section we discuss the evidence that supports the model in Figure 11, which shows how microtubules extending along the cortex support plasma membrane-bound, disk-like septin assemblies in nonadhered cells.

### Septin-reporter caveats

Fungal and animal septin core heteromers resist dissociation in high salt and characterization of recombinant septin heteromers suggests that the assembly is cotranslational (reviewed in McMurray and Thorner [2009]). In addition, attempts to assemble heteromers by combining individual recombinant septin subunits in a test tube have failed (Kinoshita, 2003a). However, there is still ample evidence for subunit exchange within core heteromers during cell cycle and developmental transitions of budding yeast, which suggests that this organism has chaperones or other factors facilitating subunit exchange (McMurray and Thorner, 2008). To address premises for tagging the endogenous mammalian heteromer pool with AcGFP reporters, we monitored the assembly states of epitope-tagged SEPT7 (Figure 1) or SEPT2 and SEPT6 (unpublished data) following a pulse of their expression. Our data support the notion that mammalian core heteromers are stable protein complexes and that heterooligomerization of tagged septins occurs only during de novo synthesis.

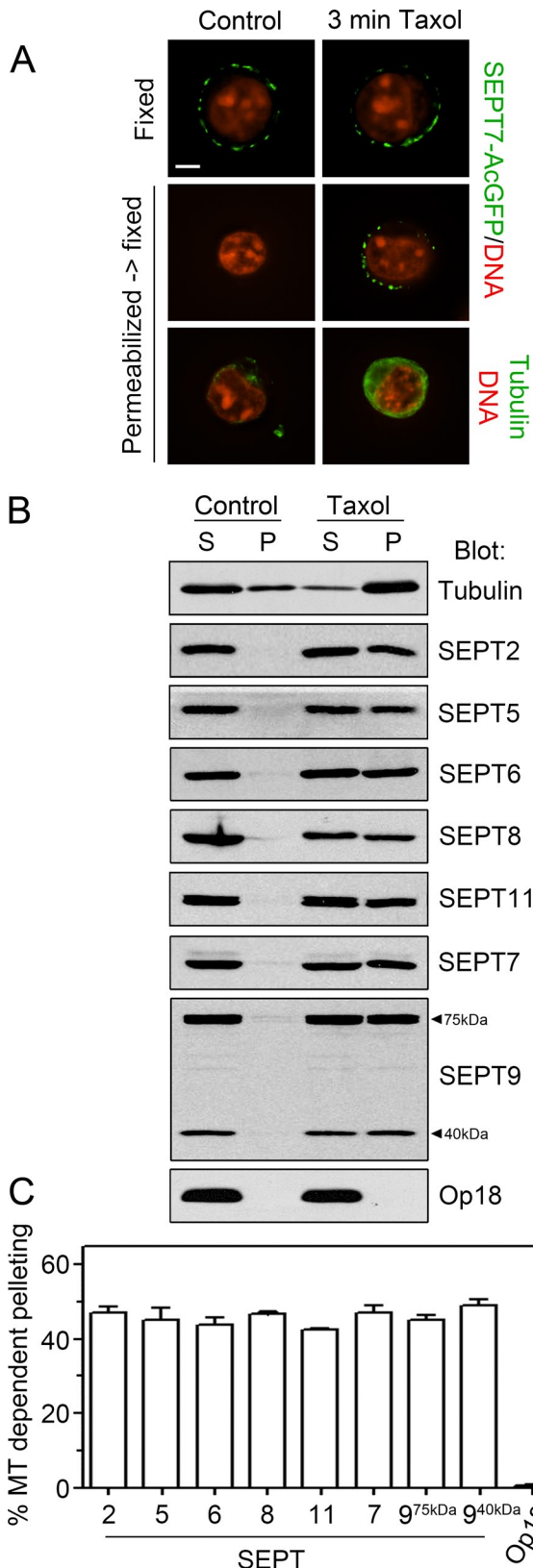


**FIGURE 7:** The effect of a brief Taxol exposure on the stability of septin disks in permeabilized cells. (A) SEPT7-AcGFP-expressing K562 cells (generated as in Figure 2) were either untreated (Control) or Taxol-treated (3  $\mu$ M; 3 min). Cells were thereafter either paraformaldehyde-fixed (top panels) or permeabilized as outlined in *Materials and Methods* prior to fixation. Microtubules in untransfected permeabilized cells were analyzed by immunostaining

Studies of K562, Jurkat, and HeLa cells suggest that endogenous septins exist solely in the context of six- to eight-subunit core heteromers (Sellin *et al.*, 2011). Despite optimized conditions for heterooligomerization with endogenous septins, only SEPT7 reporters were effectively integrated into core heteromers. It is also noteworthy that both the SEPT2- and SEPT6-reporters are prone to form ectopic filaments, which were found to sequester endogenous heteromers and thereby deplete the native cortical assemblies (Figure S3). Thus, if expressed at nonphysiological levels, these septins are promiscuous with respect to pairing partners, which is indeed as predicted by oligomerization of bacterially expressed septins (Sheffield *et al.*, 2003). This puts previous work based on septin reporters into perspective, since septin localization may not represent the localization of endogenous core heteromers. These issues are expanded on and further discussed in the Supplemental Material.

### Microtubule-supported organization of submembranous closed septin filaments

The most common higher-order septin arrangement across kingdoms is a circular structure in the size range  $\varnothing$  0.5–3.5  $\mu$ m, which is thought to function in scaffolds and/or lateral diffusion barriers in both fungi and animals (reviewed in Gladfelter [2010]). Moreover, hyphal fungi contain several distinct classes of circular septin structures in a single cell (DeMay *et al.*, 2009). Significantly, actin filament-disrupting drugs cause transformation of the actin bundle-associated septins observed in fibroblasts into free-floating circles ( $\varnothing$  ~0.6  $\mu$ m; Kinoshita *et al.*, 2002; Schmidt and Nichols, 2004). It is also noteworthy that circular  $\varnothing$  ~0.6- $\mu$ m filamentous septin bundles are formed spontaneously by recombinant human SEPT2/6/7 hexamers stored under low-salt conditions (Kinoshita *et al.*, 2002). Thus there is ample evidence to suggest that mammalian heteromers have an innate propensity to assemble into  $\varnothing$  0.6- to 0.8- $\mu$ m continuous filamentous hoops. The  $\varnothing$  ~0.8- $\mu$ m structure characterized in this study appears as a disk attached flat against the plasma membrane, many of these structures have a visible central clearing (Figures 3, 8, and S4A). These disks are distinguished from previously described circular structures in animal cells by an exclusive cortical localization and microtubule dependence.

Previous reports on interacting microtubule and septin systems (reviewed in Spiliotis [2010]) provoked the initiation of the present study. On the basis of our experiences in studies on MAP4 (reviewed in Holmfeldt *et al.* [2009]), we have evaluated previously reported links between MAP4 and septins. However, we have failed to detect any functional links (Figures S6 and S7) or interactions between these proteins (unpublished data). Moreover, while microtubule depolymerization or tubulin heterodimer depletion caused dispersal of septin disks (Figures 4, 5, and 7), we did not detect any effect on the microtubule system caused

(bottom panels). Owing to a dense microtubule array, individual microtubules are not clearly resolved. Deconvoluted optical sections at the equatorial plane of representative cells are shown. DNA (red fluorescence) was stained by propidium iodide. Scale bar: 5  $\mu$ m. (B) K562 cells were either untreated (Control) or Taxol-treated for 3 min and subsequently permeabilized, as in (A). The released supernatant (S) and cell-associated (pellet [P]) proteins were analyzed by Western blotting. The cytosolic Op18 protein served as control for complete permeabilization in the presence of Taxol. (C) The fraction of individual septins that remained cell-associated in Taxol-treated cells was determined by quantification of Western blots. Bar charts represent the mean  $\pm$  SE of data from duplicate experiments.

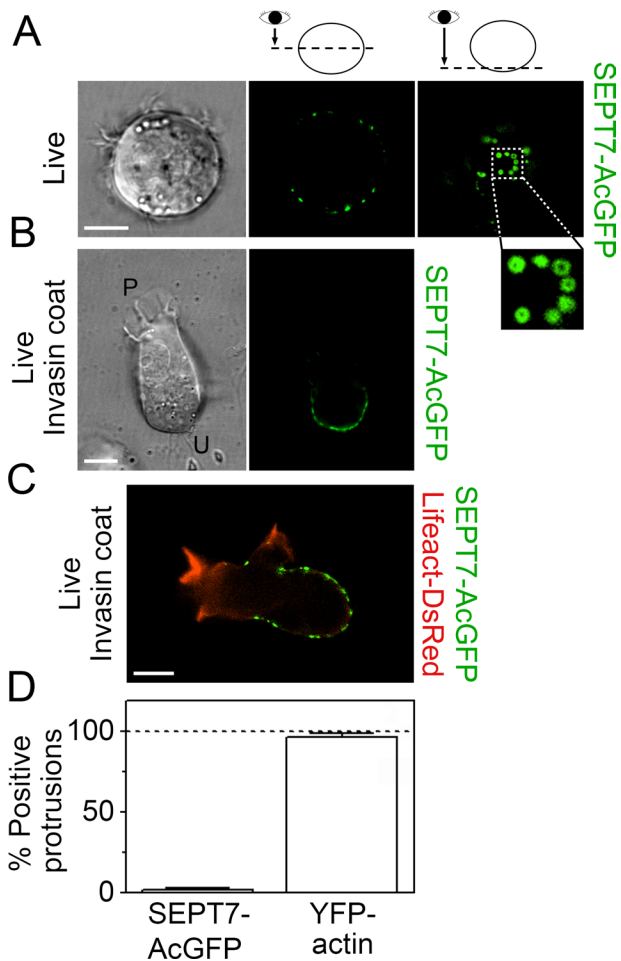


**FIGURE 8:** Analyses of septin assemblies in nonadherent or migrating T lymphocytes. (A) A phase-contrast image (left) or deconvoluted optical sections at the equatorial plane (middle) and parallel to the plasma membrane (right) of albumin-plated (i.e., nonadherent) SEPT7-AcGFP-expressing Jurkat cells are shown. This cell line was generated by the same general strategy as described for K562 cells in Figure 2. (B) Same as (A), but cells were plated onto an invasin-coated surface. The uropod (U) and surface-attached pseudopodium (P) are indicated. (C) An overlay image of an invasin-plated Jurkat cell that coexpresses the actin-filament marker Lifeact-DsRed monomer (red) and SEPT7-AcGFP (green). Coinciding red and green fluorescence signals (manifested as yellow) are not detected, which imply spatial separation. Scale bars in (A to C): 5  $\mu$ m. (D) Protrusions of invasin-plated Jurkat cells, as detected by phase-contrast microscopy, were scored for the presence of detectable septin assemblies, as revealed by the SEPT7-AcGFP reporter. For comparison, the corresponding analysis of YFP-actin-expressing Jurkat cells is also shown, which reveals that essentially all protrusions are readily visualized by the YFP-actin reporter. In each case, all protrusions in 25 cells were analyzed in duplicate experiments.

by depletion of septins (Figures 5 and S6) or excessive overexpression of SEPT2 (Figure S7). However, we noted accumulation of septins on microtubule bundles in long-term Taxol-treated cells, which suggests an innate propensity of septins to bind microtubules or associated proteins (Figures 6 and S8). Such an innate propensity seems generally consistent with studies on cells containing bundles in a native context. For example, in platelets (anuclear blood cells), septins localize to a densely packed circumferential cortical coil of microtubules (Martinez *et al.*, 2006).

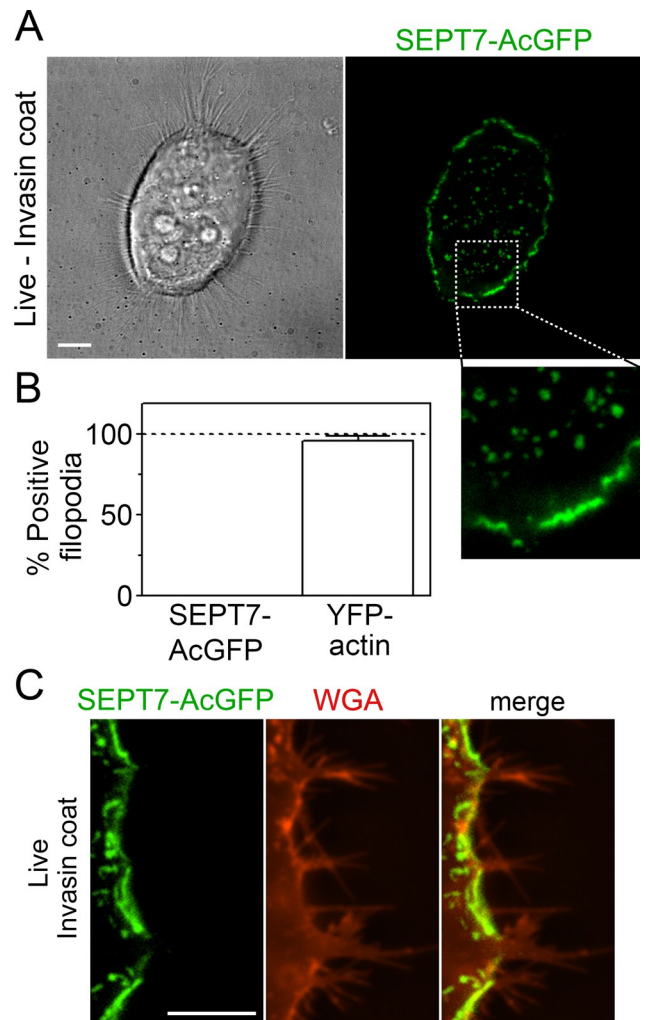


**FIGURE 9:** Septin assemblies observed in K562-KA8 cells spreading on an invasin-coated surface. A SEPT7-AcGFP-expressing K562-KA8 cell line was generated by the same general strategy as described for parental K562 cells in Figure 2. Cells were plated onto an invasin-coated surface for ~1 h. (A) A phase-contrast image (left) and a deconvoluted optical section parallel to the attachment substrate (right) of a living cell is shown. The enlargement shown below the right panel reveals heterogeneous septin assemblies. (B) Filopodia of invasin-plated K562-KA8 cells were scored for the presence of detectable septin or actin assemblies as in Figure 8D. (C) To visualize the outside of the plasma membrane by red fluorescence, Alexa Fluor 594-WGA (a sialic acid-binding lectin) was added to live cells, and the image was captured within 5 min. Left, localization of SEPT7-AcGFP; middle, the plasma membrane; right, an overlay of red and green fluorescence. Scale bars: 5  $\mu$ m.

Septins also appear to interact with the perinuclear microtubule bundles observed during the microtubule remodeling process that is a hallmark of epithelial polarization (Bowen *et al.*, 2011). Moreover, under sporulation-promoting conditions, septins also colocalize with microtubules in budding yeast (Pablo-Hernando *et al.*, 2008). Finally, while septins do not localize to the mitotic spindle of K562 or Jurkat cells (Figure S4D; unpublished data), septins do appear to colocalize with densely arranged microtubules during metaphase as well as in the final phases of cytokinesis in other cell types (Surka *et al.*, 2002; Spiliotis *et al.*, 2005; Zhu *et al.*, 2008).

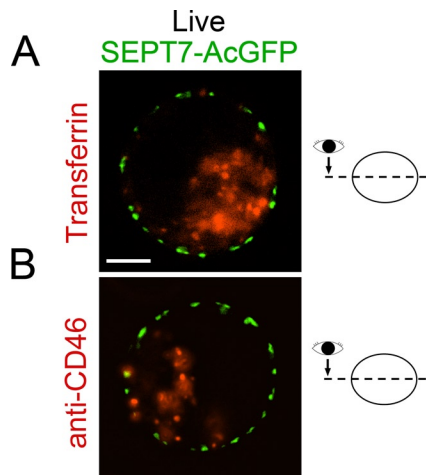


**FIGURE 10:** Internalization of plasma membrane proteins by nonadherent K562 cells. Internalization at 37°C was analyzed by addition of the indicated red fluorescence-labeled, cell surface-binding ligand to K562 cells. (A and B) Overlays of deconvoluted optical sections at the equatorial plane of representative SEPT7-AcGFP-expressing cells (A) Internalized Alexa Fluor 594-labeled transferrin after 10-min incubation. (B) Internalization of cross-linked CD46 was scored by precoating with anti-CD46 (a monoclonal mouse antibody) for 40 min, after which cells were washed and then incubated with DyLight 549-labeled secondary antibodies (polyclonal goat anti-mouse). An image captured after 30 min is shown, and it is evident that essentially all immune complexes were already internalized at this time point. Scale bar: 5  $\mu$ m.

Septins colocalize with actin bundles at the contractile ring during cytokinesis and at stress fibers during interphase; both processes depend on specific adaptors (Kinoshita *et al.*, 2002). Thus, as evidenced by their localization in intact cells, septins have an apparent innate propensity to bind densely arranged assemblies of either microtubules or actin. Moreover, purified septin heteromers of both yeast and mammalian origins are known to interact with PIP2. This is a compartmentalized phosphoinositide enriched at the inner leaflet of the plasma membrane (reviewed in Varnai and Balla [2007]), which promotes polymerization and organization of purified heteromers on artificial lipid layers (Tanaka-Takiguchi *et al.*, 2009; Bertin *et al.*, 2010). Thus PIP2 interactions may at least in part explain the propensity of septins to localize to the plasma membrane of K562 and Jurkat cells.

It is noteworthy that, while septin disks in nonadherent cells depend on intact microtubules, the diffuse array of minute septin assemblies observed in microtubule-deficient cells are still retained at the plasma membrane (Figure 4). These observations provide the foundation for the model depicted in Figure 11. Thus densely arranged microtubules that extend along the cortex, such as in spherical adhesion substrate-independent cells (Figure 4A), may provide sufficient multiple-bond interactions to cooperate with binding sites at the plasma membrane, such as PIP2, and thereby facilitate assembly into septin disks. In addition, septin localization during cytokinesis of mammalian cells may also be facilitated by an analogous mechanism, namely cooperative binding at the plasma membrane and a septin adaptor such as anillin, which appears to interact with both septins and actin bundles at the contractile ring (Oegema *et al.*, 2000; Kinoshita *et al.*, 2002). In contrast, as shown here, actin filaments involved in remodeling of the plasma mem-

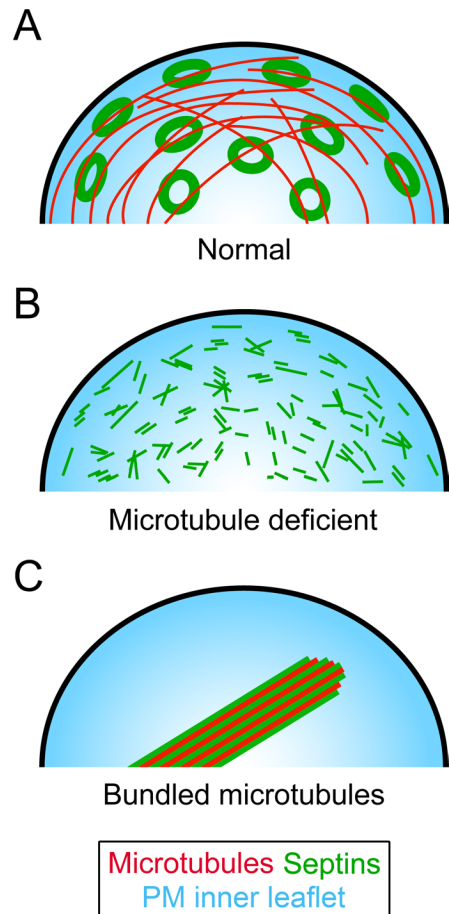


**FIGURE 11:** A model of the significance of cooperative and/or multivalent interactions for the localization and arrangement of septins. A part of the inner leaflet of the plasma membrane of a spherical cell, e.g., a nonadherent cell type of hematopoietic origin, is depicted (a half-circle representing an inside view of a quarter-sphere). Blue represents the inner leaflet of the plasma membrane. (A) A nonadherent cell has densely arranged microtubules (red lines) extending along the cortex (see images in Figure 4A). Microtubule-supported  $\approx 0.8\text{-}\mu\text{m}$  septin disks (depicted as green circles) are attached flat against the plasma membrane. The model predicts cooperation between multivalent binding of ligands, such as PIP2, at the inner leaflet of the plasma membrane and cortical microtubules (red) to each side of individual septin disks. In analogy to septin binding to actin filaments, microtubule binding may depend on an adaptor. (B) Heterogeneous green symbols represent a diffuse array of minute septin assemblies all around the cortex, i.e., as observed in cells lacking microtubules. Given previous demonstrations of PIP2-dependent assembly of septins on artificial lipid layers, the exclusive plasma membrane proximal localization may at least in part depend on PIP2 interactions. (C) Bundling of microtubules (red lines) can be envisioned as providing favorable multiple-bond interaction. The salient point of this model is that septins can be expected to assemble at locations that provide the greatest opportunity for binding cooperativity, which depends on both the cell type and external cues, such as integrin signaling. It follows that the plasma membrane-associated septin assemblies, which are well-documented across kingdoms, may become depleted by sequestering onto bundles of either microtubules or actin filaments under certain physiological and/or experimental conditions.

brane during interphase (such as within filopodia or pseudopodia) are mutually exclusive with septin assemblies (Figures 8 and 9).

## Evidence that submembranous septin assemblies delineate static plasma membrane regions

Cortical septin disks are the predominant septin assemblies detected in cells lacking substrate attachment (Figures 3 and S4). This, combined with preservation by microtubule stabilization, allowed us to address their composition by Western blotting (Figure 7). The data suggested that all the expressed septins are equally represented, and we obtained no evidence for a variable dependence on specific septins between cell types (Figures 7C, S9, and S10). Analysis of Taxol-treated cells permeabilized over a 5- to 60-min time period revealed only a slow decay of cell-associated septin structures (unpublished data). Given that this analysis implied a dramatic dilution at physiological ionic strength, ~50% of insoluble septins may still represent an underestimate of the fraction of core heteromers assembled into cortical disks.

A K562 cell contains ~180,000 heteromers (~0.1% of total cell proteins, of which approximately two-thirds is six-subunit and one-third is eight-subunit heteromers; Sellin *et al.*, 2011). This number should be compared with  $\sim 1 \times 10^7$  tubulin heterodimers in a K562 cell (~2% of total cell proteins; Sellin *et al.*, 2008a), which implies an ~60-fold molar excess of tubulin heterodimers over septin heteromers. Based on the assumption that most heteromers are assembled into  $141 \pm 29$  septin disks per cell (Figure S4C), it can be deduced that each one contains ~1300 heteromers. Moreover, given an average cell surface area of  $850 \mu\text{m}^2$  (depending on cell cycle stage; Figure S4B) and that each septin disk covers a  $\sim 0.5\text{-}\mu\text{m}^2$  area, these disks occupy roughly 8% of the inner leaflet of the plasma membrane of nonadhered, blood-derived cell types such as K562.

Each septin disk occupies a much larger area than any known functional unit in the plasma membrane of animal cells; in most cases, these areas are referred to as "microdomains" (Lingwood and Simons, 2010). These are most often described as dynamic domains smaller than the resolution of light microscopy, which contrast to the readily resolved septin assemblies that appear mutually exclusive with membrane remodeling events. Thus analysis of various plasma membrane remodeling events in living K562 or Jurkat cells indicated exclusion of all detectable septin assemblies from dynamic regions of the plasma membrane (Figures 8–10).

As depicted in Figure 11, our results indicate that the septin-disk arrangement depends on cortical microtubules, which are densely arranged along the cortex of nonadhered spherical cells such as K562 and Jurkat (Figure 4A; Holmfeldt *et al.*, 2003a). Such multivalent microtubule interactions combined with cooperative binding at the inner leaflet of the plasma membrane are likely to be of significance for the static nature of cortical septin disks. In the case of the septin arrangements observed in cells adhered to a substrate or during cell division, the model in Figure 11 predicts that other types of multivalent interactions will provide static properties to higher-order septin structures.

## Concluding remarks

During amoeboid movement of Jurkat T lymphocytes we found that punctuate septin assemblies accumulate at the cortex of the trailing uropod (Figure 8). This appears generally consistent with published images of immunostained murine T lymphocytes (Tooley *et al.*, 2009), which shows a mix of fibrous and punctuate septins at the uropod cortex. It was stated by the authors that the appearance of septin assemblies varies considerably with the antibody used for detection, and it was specifically noted that in some cells, particularly for detection of Sept6, distributions are predominantly punctuate. Based on the observed cortical localization and enhanced migration of septin-depleted cells through restrictive pores in trans-well

assays (Tooley *et al.*, 2009), it was proposed that septin assemblies provide cortical rigidity. However, we have not found that septin depletion of Jurkat T lymphocytes (by means of shRNA-SEPT7 expression; see Figure 5A), facilitates trans-migration through restrictive pores (3- and 5- $\mu\text{m}$  pores tested, with or without chemoattractant [unpublished data]). Moreover, we have not detected fibrous septins in the uropod. Thus our observations do not support the idea of a rigidifying "septin corset" at the uropod cortex that consists of fibers oriented perpendicular to the axis of locomotion.

Our studies on K562 and Jurkat cells cannot be directly compared with the inherently polarized cells of budding yeast, that is, the model system in which the significance of septins for membrane dynamics at the bud site has been established. It is still noteworthy that the actin cables that guide vesicle transport into the emerging bud have been shown to be spatially segregated from the septin ring structure that initially marks the bud site and thereafter remain at the base of the bud as a diffusion barrier and scaffold (reviewed in Oh and Bi [2011]). An analogous sequence of events has been observed in hyphal fungi in which the diffuse septin patch at the hyphal tip is transformed to a ring encircling the hyphal cell cortex (reviewed in Gladfelter [2010]). Studies of dendritic spines, flagellum, and cilia in vertebrates also reveal septin assemblies confined to the base of cell appendages (Ihara *et al.*, 2005; Kissel *et al.*, 2005; Tada *et al.*, 2007; Xie *et al.*, 2007; Hu *et al.*, 2010). At this location, septins across kingdoms appear to function as a lateral diffusion barrier, which implies both static features and lateral immobility. Thus our evidence that submembranous septin assemblies in mammalian cells are mutually exclusive with dynamic membrane regions seems completely consistent with studies concerned with a diverse array of cellular structures and organisms.

## MATERIALS AND METHODS

### DNA constructs, shuttle vectors, and regulated expression from the hMTIIa promoter

Construction of EBV-based shuttle vectors directing constitutive expression of shRNA targeting mRNAs encoding SEPT2, SEPT5, SEPT7, SEPT9, Op18, and MAP4 has been described (Holmfeldt *et al.*, 2007; Sellin *et al.*, 2011). The derivative encoding shRNA-SEPT6 was constructed by an analogous strategy (accession NM\_145799.2; targeting sequence: GAGAGACAAAGAGAAGAAA). EBV-based pMEP4 shuttle vectors directing inducible expression of SEPT6-FLAG, SEPT7-FLAG, Op18-FLAG, MAP4-FLAG, and TBCE-FLAG, all of which contain a C-terminal eight-amino acid FLAG-epitope tag, as well as His-SEPT7, which contains an N-terminal 6 $\times$ His tag, have been described (Holmfeldt *et al.*, 2002; Sellin *et al.*, 2008b, 2011). The pMEP4 vector directing expression of SEPT2 derivative with an eight amino acid FLAG (SEPT2-FLAG) was constructed by an analogous PCR-based strategy using pK-myc-SEPT2 (NP\_001008492.1) as a template (Sheffield *et al.*, 2003). Vectors directing expression of septins fused at their C-terminus with AcGFP were based on either the pMEP4 or pCEP4 shuttle vectors, as indicated in text. The SEPT2-, SEPT6-, SEPT7- and SEPT9-AcGFP (SEPT9\_v1-transcript; Nagata *et al.*, 2003) derivatives have the same general design and include the complete open reading frames, with AcGFP located at the C-terminus. Constructions of these reporters, as well as the Lifeact-DsRed monomer reporter (Riedl *et al.*, 2008), are detailed in the Supplemental Material. The general procedure for transfections of K562 or Jurkat with shuttle vectors and subsequent selection of hygromycin has been described (Holmfeldt *et al.*, 2007). A transient burst of maximum expression from the hMTIIa promoter of pMEP4, which peaks during the first 6- to 8-h period of stimulation, was achieved by shifting cells from a medium designed

to suppress expression (containing 25  $\mu\text{M}$  EDTA) to a medium containing 0.25  $\mu\text{M}$   $\text{CdCl}_2$  (Melander Gradin *et al.*, 1997; Sellin *et al.*, 2008a). Constitutive expression from the hMTIIa promoter was obtained by cultivation of cells in standard growth medium (RPMI 1640 supplemented with insulin, 5 mg/l, transferrin, 5 mg/l, sodium selenite, 5  $\mu\text{g/l}$ , and 5% fetal calf serum). Co-transfections of pCEP4, pMEP4, and/or shRNA vectors were performed as described (Melander Gradin *et al.*, 1997; Holmfeldt *et al.*, 2004).

### Immunoblotting, antibodies, and determination of tubulin monomer–polymer partitioning

Immunoblotting and subsequent detection using the ECL detection system (GE Healthcare, Waukesha, WI) were performed using Op18, MAP4,  $\alpha$ -tubulin, HSP70, and FLAG-tagged antibodies described in Holmfeldt *et al.* (2002) and the panel of septin antibodies described in Sellin *et al.* (2011). Moreover, antibodies toward GFP (sc-9996; Santa Cruz Biotechnology, Santa Cruz, CA), CD46 (555948; PharMingen, BD Biosciences, San Diego, CA), and SEPT8 (sc-48937; Santa Cruz Biotechnology) were also used. For quantitative analysis of Western blots, the Bio-Rad ChemiDoc (Bio-Rad, Hercules, CA) system was used with the Quantity One 4.4 program. Microtubule content was determined as detailed in Sellin *et al.* (2008a). To determine the total amount of polymerizable tubulin, cells were treated with the polymerization-promoting drug Taxol (15 min, 2  $\mu\text{g/ml}$ ), which was found by quantitative Western blotting to cause essentially complete polymerization (<3% unassembled tubulin) and allowed calculation of tubulin heterodimer–polymer partitioning.

### Determinations of protein partitioning between soluble and cell-associated states, and hydrodynamic parameters

The assembly state of septins was evaluated by an assay based on the release of soluble septins after cell permeabilization (Sellin *et al.*, 2011). In brief, cells were gently resuspended in the presence of 0.2% saponin, 10  $\mu\text{g/ml}$  leupeptin in 80 mM PIPES (pH 6.9), 2 mM  $\text{MgCl}_2$ , and 4 mM ethylene glycol tetraacetic acid (PEM buffer [80 mM PIPES, pH 6.9, 2 mM  $\text{MgCl}_2$ , 4 mM ethylene glycol tetraacetic acid]). The particulate cell fraction was isolated by centrifugation (0.5 min, 2000  $\times g$ ). Proteins in the pellet (i.e., the cell-associated insoluble fraction) and supernatant (i.e., released soluble cellular proteins) were resolved by 12.5% SDS–PAGE and quantified by Western blotting. In the absence of a microtubule-stabilizing agent such as Taxol, the supernatant contained > 95% of all septins (Sellin *et al.*, 2011). Prior to analysis of hydrodynamic parameters, the supernatant of permeabilized cells was supplemented with 0.5 M NaCl, which results in complete disassembly of septins into six- and eight-subunit core heteromers (Sellin *et al.*, 2011). Density-gradient centrifugation, gel-filtration chromatography, and calculation of molecular masses were performed as described in Sellin *et al.* (2011).

### Examination of live or fixed cells by fluorescence microscopy

Cells were cultivated in chamber slides (100  $\mu\text{l/well}$ ; LabTek II; Nalge Nunc International, Naperville, IL) coated with BSA or with the bacterial *Yersinia pseudotuberculosis* invasin protein at 10  $\mu\text{g/ml}$  (Arencibia *et al.*, 1997). Epifluorescence images were acquired on an Olympus CellR imaging station (Olympus Biosystems, Planegg, Germany) equipped with an inverted microscope (IX81; Olympus), a 100 $\times$  1.4 numerical aperture Plan apochromat objective, and a cooled CCD camera (Orca ER; Hamamatsu Photonics, Herrsching am Ammersee, Germany). Microscopy of live cells was performed at 37°C (humidified air with 5%  $\text{CO}_2$ ). Immunostaining of cells was performed after fixation in either 2% paraformaldehyde (37°C) or methanol (–20°C) as previously described (Holmfeldt *et al.*, 2003b).

Methanol- and paraformaldehyde-based fixation protocols resulted in similar appearances of SEPT7–AcGFP visualized structures, but fixation causes blurring of septin disks, and this effect varied between experiments. All immunostaining of SEPT7 was performed on methanol-fixed cells, since the antibody fails in specificity if used in combination with paraformaldehyde fixation. As indicated in the text, some analyses involved permeabilization of cells with 0.2% saponin in PEM buffer prior to fixation, which resulted in release of soluble proteins, such as nonpolymerized septin heteromers or tubulin heterodimers. Antibodies used for immunostaining are described above and Alexa Fluor 594–labeled transferrin (T13343; Molecular Probes, Invitrogen, Carlsbad, CA), Alexa Fluor 568–labeled phalloidin (A12380; Molecular Probes, Invitrogen), and Alexa Fluor 594–labeled wheat germ agglutinin (WGA; W11262; Molecular Probes, Invitrogen) were used as fluorescent probes for live and/or fixed cells.

### ACKNOWLEDGMENTS

This work was supported by the Swedish Research Council. Special thanks to Ian G. Macara, Koh-Ichi Nagata, and Pascale Cossart for generously providing cDNA and antibody reagents.

### REFERENCES

- Arencibia I, Suarez NC, Wolf-Watz H, Sundqvist KG (1997). Yersinia invasin, a bacterial beta1-integrin ligand, is a potent inducer of lymphocyte motility and migration to collagen type IV and fibronectin. *J Immunol* 159, 1853–1859.
- Bertin A, McMurray MA, Grob P, Park SS, Garcia G, III, Patanwala I, Ng HL, Alber T, Thorner J, Nogales E (2008). *Saccharomyces cerevisiae* septins: supramolecular organization of heterooligomers and the mechanism of filament assembly. *Proc Natl Acad Sci USA* 105, 8274–8279.
- Bertin A, McMurray MA, Thai L, Garcia G, III, Votin V, Grob P, Allyn T, Thorner J, Nogales E (2010). Phosphatidylinositol-4,5-bisphosphate promotes budding yeast septin filament assembly and organization. *J Mol Biol* 404, 711–731.
- Bhamidipati A, Lewis SA, Cowan NJ (2000). ADP ribosylation factor-like protein 2 (Arl2) regulates the interaction of tubulin-folding cofactor D with native tubulin. *J Cell Biol* 149, 1087–1096.
- Bowen JR, Hwang D, Bai X, Roy D, Spiliotis ET (2011). Septin GTPases spatially guide microtubule organization and plus end dynamics in polarizing epithelia. *J Cell Biol* 194, 187–197.
- Cao L, Ding X, Yu W, Yang X, Shen S, Yu L (2007). Phylogenetic and evolutionary analysis of the septin protein family in metazoan. *FEBS Lett* 581, 5526–5532.
- Casamayor A, Snyder M (2003). Molecular dissection of a yeast septin: distinct domains are required for septin interaction, localization, and function. *Mol Cell Biol* 23, 2762–2777.
- Caudron F, Barral Y (2009). Septins and the lateral compartmentalization of eukaryotic membranes. *Dev Cell* 16, 493–506.
- DeMay BS, Bai X, Howard L, Occhipinti P, Meseroll RA, Spiliotis ET, Oldenbourg R, Gladfelter AS (2011). Septin filaments exhibit a dynamic, paired organization that is conserved from yeast to mammals. *J Cell Biol* 193, 1065–1081.
- DeMay BS, Meseroll RA, Occhipinti P, Gladfelter AS (2009). Regulation of distinct septin rings in a single cell by Elm1p and Gin4p kinases. *Mol Biol Cell* 20, 2311–2326.
- Gladfelter AS (2010). Guides to the final frontier of the cytoskeleton: septins in filamentous fungi. *Curr Opin Microbiol* 13, 720–726.
- Holmfeldt P, Brannstrom K, Stenmark S, Gullberg M (2003a). Deciphering the cellular functions of the Op18/Stathmin family of microtubule-regulators by plasma membrane-targeted localization. *Mol Biol Cell* 14, 3716–3729.
- Holmfeldt P, Brattsand G, Gullberg M (2002). MAP4 counteracts microtubule catastrophe promotion but not tubulin-sequestering activity in intact cells. *Curr Biol* 12, 1034–1039.
- Holmfeldt P, Brattsand G, Gullberg M (2003b). Interphase and monoastral-mitotic phenotypes of overexpressed MAP4 are modulated by free tubulin concentrations. *J Cell Sci* 116, 3701–3711.
- Holmfeldt P, Sellin ME, Gullberg M (2009). Predominant regulators of tubulin monomer-polymer partitioning and their implication for cell polarization. *Cell Mol Life Sci* 66, 3263–3276.

- Holmfeldt P, Stenmark S, Gullberg M (2004). Differential functional interplay of TOGp/XMAP215 and the KinI kinesin MCAK during interphase and mitosis. *EMBO J* 23, 627–637.
- Holmfeldt P, Stenmark S, Gullberg M (2007). Interphase-specific phosphorylation-mediated regulation of tubulin dimer partitioning in human cells. *Mol Biol Cell* 18, 1909–1917.
- Hu Q, Milenkovic L, Jin H, Scott MP, Nachury MV, Spiliotis ET, Nelson WJ (2010). A septin diffusion barrier at the base of the primary cilium maintains ciliary membrane protein distribution. *Science* 329, 436–439.
- Huang YW, Yan M, Collins RF, Diccio JE, Grinstein S, Trimble WS (2008). Mammalian septins are required for phagosome formation. *Mol Biol Cell* 19, 1717–1726.
- Ihara M, et al. (2005). Cortical organization by the septin cytoskeleton is essential for structural and mechanical integrity of mammalian spermatozoa. *Dev Cell* 8, 343–352.
- Kinoshita M (2003a). Assembly of mammalian septins. *J Biochem* 134, 491–496.
- Kinoshita M (2003b). The septins. *Genome Biol* 4, 236.
- Kinoshita M, Field CM, Coughlin ML, Straight AF, Mitchison TJ (2002). Self- and actin-templated assembly of mammalian septins. *Dev Cell* 3, 791–802.
- Kissel H, Georgescu MM, Larisch S, Manova K, Hunnicutt GR, Steller H (2005). The Sept4 septin locus is required for sperm terminal differentiation in mice. *Dev Cell* 8, 353–364.
- Kremer BE, Adang LA, Macara IG (2007). Septins regulate actin organization and cell-cycle arrest through nuclear accumulation of NCK mediated by SOCS7. *Cell* 130, 837–850.
- Kremer BE, Haystead T, Macara IG (2005). Mammalian septins regulate microtubule stability through interaction with the microtubule-binding protein MAP4. *Mol Biol Cell* 16, 4648–4659.
- Lindsey R, Momany M (2006). Septin localization across kingdoms: three themes with variations. *Curr Opin Microbiol* 9, 559–565.
- Lingwood D, Simons K (2010). Lipid rafts as a membrane-organizing principle. *Science* 327, 46–50.
- Martinez C, Corral J, Dent JA, Sesma L, Vicente V, Ware J (2006). Platelet septin complexes form rings and associate with the microtubular network. *J Thromb Haemost* 4, 1388–1395.
- McMurray MA, Bertin A, Garcia G, III, Lam L, Nogales E, Thorner J (2011). Septin filament formation is essential in budding yeast. *Dev Cell* 20, 540–549.
- McMurray MA, Thorner J (2008). Septin stability and recycling during dynamic structural transitions in cell division and development. *Curr Biol* 18, 1203–1208.
- McMurray MA, Thorner J (2009). Reuse, replace, recycle. Specificity in subunit inheritance and assembly of higher-order septin structures during mitotic and meiotic division in budding yeast. *Cell Cycle* 8, 195–203.
- Melander Gradin H, Marklund U, Larsson N, Chatila TA, Gullberg M (1997). Regulation of microtubule dynamics by Ca<sup>2+</sup>/calmodulin-dependent kinase IV/Gr-dependent phosphorylation of oncoprotein 18. *Mol Cell Biol* 17, 3459–3467.
- Mostowy S et al. (2010). Entrapment of intracytosolic bacteria by septin cage-like structures. *Cell Host Microbe* 8, 433–444.
- Muller U, Bossy B, Venstrom K, Reichardt LF (1995). Integrin alpha 8 beta 1 promotes attachment, cell spreading, and neurite outgrowth on fibronectin. *Mol Biol Cell* 6, 433–448.
- Nagata K et al. (2003). Filament formation of MSF-A, a mammalian septin, in human mammary epithelial cells depends on interactions with microtubules. *J Biol Chem* 278, 18538–18543.
- Oegema K, Savoian MS, Mitchison TJ, Field CM (2000). Functional analysis of a human homologue of the *Drosophila* actin binding protein anillin suggests a role in cytokinesis. *J Cell Biol* 150, 539–552.
- Oh Y, Bi E (2011). Septin structure and function in yeast and beyond. *Trends Cell Biol* 21, 141–148.
- Pablo-Hernando ME, Arnaiz-Pita Y, Tachikawa H, del Rey F, Neiman AM, Vazquez de Aldana CR (2008). Septins localize to microtubules during nutritional limitation in *Saccharomyces cerevisiae*. *BMC Cell Biol* 9, 55.
- Pan F, Malmberg RL, Momany M (2007). Analysis of septins across kingdoms reveals orthology and new motifs. *BMC Evol Biol* 7, 103.
- Peterson EA, Petty EM (2010). Conquering the complex world of human septins: implications for health and disease. *Clin Genet* 77, 511–524.
- Riedl J et al. (2008). Lifeact: a versatile marker to visualize F-actin. *Nat Methods* 5, 605–607.
- Schmidt K, Nichols BJ (2004). Functional interdependence between septin and actin cytoskeleton. *BMC Cell Biol* 5, 43.
- Sellin ME, Holmfeldt P, Stenmark S, Gullberg M (2008a). Global regulation of the interphase microtubule system by abundantly expressed Op18/Stathmin. *Mol Biol Cell* 19, 2897–2906.
- Sellin ME, Holmfeldt P, Stenmark S, Gullberg M (2008b). Op18/Stathmin counteracts the activity of overexpressed tubulin-disrupting proteins in a human leukemia cell line. *Exp Cell Res* 314, 1367–1377.
- Sellin ME, Sandblad L, Stenmark S, Gullberg M (2011). Deciphering the rules governing assembly order of mammalian septin complexes. *Mol Biol Cell* 22, 3152–3164.
- Sheffield PJ, Oliver CJ, Kremer BE, Sheng S, Shao Z, Macara IG (2003). Borg/septin interactions and the assembly of mammalian septin heterodimers, trimers, and filaments. *J Biol Chem* 278, 3483–3488.
- Sirajuddin M, Farkasovsky M, Hauer F, Kuhlmann D, Macara IG, Weyand M, Stark H, Wittinghofer A (2007). Structural insight into filament formation by mammalian septins. *Nature* 449, 311–315.
- Sirajuddin M, Farkasovsky M, Zent E, Wittinghofer A (2009). GTP-induced conformational changes in septins and implications for function. *Proc Natl Acad Sci USA* 106, 16592–16597.
- Spiliotis ET (2010). Regulation of microtubule organization and functions by septin GTPases. *Cytoskeleton (Hoboken)* 67, 339–345.
- Spiliotis ET, Kinoshita M, Nelson WJ (2005). A mitotic septin scaffold required for mammalian chromosome congression and segregation. *Science* 307, 1781–1785.
- Surka MC, Tsang CW, Trimble WS (2002). The mammalian septin MSF localizes with microtubules and is required for completion of cytokinesis. *Mol Biol Cell* 13, 3532–3545.
- Tada T, Simonetta A, Batterton M, Kinoshita M, Edbauer D, Sheng M (2007). Role of septin cytoskeleton in spine morphogenesis and dendrite development in neurons. *Curr Biol* 17, 1752–1758.
- Tanaka-Takiguchi Y, Kinoshita M, Takiguchi K (2009). Septin-mediated uniform bracing of phospholipid membranes. *Curr Biol* 19, 140–145.
- Tooley AJ, Gilden J, Jacobelli J, Beemiller P, Trimble WS, Kinoshita M, Krummel MF (2009). Amoeboid T lymphocytes require the septin cytoskeleton for cortical integrity and persistent motility. *Nat Cell Biol* 11, 17–26.
- Varnai P, Balla T (2007). Visualization and manipulation of phosphoinositide dynamics in live cells using engineered protein domains. *Pflugers Arch* 455, 69–82.
- Vega IE, Hsu SC (2003). The septin protein Nedd5 associates with both the exocyst complex and microtubules and disruption of its GTPase activity promotes aberrant neurite sprouting in PC12 cells. *Neuroreport* 14, 31–37.
- Weirich CS, Erzberger JP, Barral Y (2008). The septin family of GTPases: architecture and dynamics. *Nat Rev Mol Cell Biol* 9, 478–489.
- Vrabiou AM, Mitchison TJ (2006). Structural insights into yeast septin organization from polarized fluorescence microscopy. *Nature* 443, 466–469.
- Xie Y, Vessey JP, Konecna A, Dahm R, Macchi P, Kiebler MA (2007). The GTP-binding protein septin 7 is critical for dendrite branching and dendritic-spine morphology. *Curr Biol* 17, 1746–1751.
- Zhang J, Kong C, Xie H, McPherson PS, Grinstein S, Trimble WS (1999). Phosphatidylinositol polyphosphate binding to the mammalian septin H5 is modulated by GTP. *Curr Biol* 9, 1458–1467.
- Zhu M et al. (2008). Septin 7 interacts with centromere-associated protein E and is required for its kinetochore localization. *J Biol Chem* 283, 18916–18925.